4. Beamline

This section describes the activity status of the light source and optics of the beamlines in FY2018. It includes the insertion device, frontend, optics and transport channel, radiation shielding of SPring-8, and SACLA beamlines. In addition to routine maintenance, several component upgrades and R&D were performed. Some of these endeavors were part of the SPring-8 major upgrade.

We also began rearranging the beamline portfolio. BL45XU was fully remodeled with regard to the insertion device, optics, and end station due to the increased demand for PX crystallography in this fiscal year.

1. Insertion device and frontend

1-1. Insertion device

As part of the renewal of the existing beamlines in preparation for the upcoming major upgrade of the storage ring, where the straight section will be shortened, replacement of existing insertion devices (IDs) has been ongoing since FY2016. In FY2018, two in-vacuum undulators (IVUs) for BL10XU and BL45XU, which have been operational for more than 20 years, were replaced with new ones.

The new ID for BL10XU is an IVU based on a new concept: magnetic force cancellation using multipole monolithic magnets and modular magnetic arrays to facilitate the field correction process, which is indispensable for high-quality IDs. Both of these offer efficient and cost-effective ways to manufacture IVUs, which is critically important in the SPring-8 upgrade project. The research and development to demonstrate this concept have been conducted for several years. After constructing and testing a few prototype devices, the first practical device that is compatible with the stable operation of the storage ring was built and installed in the 34 cells of the SPring-8 storage ring. After the beam test to verify the performance as an IVU, it was moved to the 10 cells to be operated as the new ID for BL10XU.

As for BL45XU, where a pair of vertically polarized IVUs have been running since 1997, a new (horizontally polarized) IVU was constructed by refurbishing an existing standard IVU. Although most of the specifications are the same, the total length has been reduced from 4.5 m to 3.0 m to ensure compatibility with future upgrades of the storage ring. This is possible because the standard IVU is composed of three 1.5-m long units (*i.e.,* three magnetic arrays and three vacuum chambers mechanically connected with each other and mounted on a common base made of steel). Thus, by truncating one third of the common base and removing one of the three units, the IVU can be restructured as a 3.0-m long IVU. After rearranging basic components such as the end-correction magnets and cooling water channels, the new IVU was installed as the new ID for BL45XU.

1-2. Front-end

(1) Fast closing shutter (FCS)

To predict vacuum deterioration quantitatively at the most upstream of the front-end assuming that a rapture of windows and subsequent inrush of air might occur in the beamline, we have been conducting R&D on the performance evaluation of the FCS system. The effective leak of the FCS at the inrush of air can be presented as a function of the total internal volume, which allows the number of

gas molecules flowing into the most-upstream of the front-end to be estimated [1].

(2) X-ray beam position monitor (XBPM)

The filling pattern dependency of the XBPM outputs was systematically estimated for five several-bunch modes based on the beam axis in the multi-bunch mode. In the 2/29-filling + 26 bunches mode, maximum displacements of about 40 μm and 20 μm RMS were observed in the horizontal and vertical directions, respectively. The main cause was the space charge effect during photoemission. We successfully reduced the filling pattern dependency to less than half of the initial state through the following measures: (i) centering the detector heads to the beam axis, (ii) widening the ID gap for fixed-point observations, and (iii) increasing the applied voltage of the collecting electrodes.

(3) New beam profile monitoring system for X-ray beam exiting from the front-end

Previous studies have demonstrated that visualizing the monochromatic beam profile while addressing the thermal issue is indispensable. Hence, the centroid of a small photon beam exiting from the front-end should be monitored. We conducted a verification experiment at BL13XU for the visualization of scattered X-ray from a thin diamond film with the pin-hole camera technique and subsequently measured the photon energy with energy-dispersive two-dimensional detectors such as SOPHIAS-L.

(4) High-heat-load handling techniques

As part of the investigations into the thermal limitation of the high-heat-load components, the dislocation densities of Glidcop with compressive strain (0.7–5.5%) applied at 100 °C were evaluated by X-ray line profile analyses with a two-dimensional flat panel detector. This realized a more detailed diffraction profile. Consequently, Fourier analysis showed that dislocation densities were 3.5×10^{14} m^{-2} – 7.1×10^{14} m^{-2}.

2. Optics and transport channel

2-1. Improvement in the stability and maintenance of double-crystal monochromators

The two double-crystal monochromators (DCMs) of BL37XU and BL46XU were remodeled to stabilize the vibrations. Since the tilt stages for the first crystals were redundant for liquid nitrogen–cooled silicon crystals, they were replaced with metal blocks. The transport paths of liquid nitrogen, which had led to both crystals in series with half-inch flexible tubes, were branched in the DCMs to flow into the first and second crystals separately. The tube diameters for the first crystals remained the same, but the diameters for the second crystals were changed to a quarter inch. The flow rates for the second crystals were reduced accordingly, and vibrations of the tubes were expected to lessen. In addition, the second tilt stage in the BL46XU DCM was replaced with a more rigid one and wider guide rails. Performance tests are scheduled for the beginning of FY2019.

Stability tests were carried out at ten operated beamlines. Vibrations of the DCMs were estimated from the intensity fluctuations of the X-ray beams at the experimental stations. By measuring the intensity fluctuations and beam positions simultaneously, we verified that the instability of the light sources partially contributed to the intensity fluctuation. Crystal deformation by the heat load was detected through distortions in the intensity and phase distributions of the X-ray beams. To quantify the deformations, we are improving estimation methods with the aid of computer

simulation.

Regular maintenance was carried out for the cooling systems with liquid nitrogen and four DCMs (BL01B1, BL20B2, BL32XU, and BL47XU). Since several motors of the BL01B1 DCM deteriorated due to aging, all the motors were replaced with new ones.

2-2. Improvement in environments of the optics hutches at HX beamlines

The standard pumping unit in the transport channel of HX-BLs is constituted by a turbo molecular pump (TMP) and a rough exhaust pump. An ion pump (IP) was integrated as the main pump to the transport channel in five BLs (BL32B2, BL13XU, BL19LXU, BL29XU, and BL41XU) to reduce vibrations, noise, and heating in the optics hutches as well as operation cost. In FY2018, IPs were newly installed at BL46XU and BL45XU. These optics hutches (OHs) were fully cleaned up. Additionally, a no shoe policy was adopted to reduce particle contamination.

2-3. Reconstruction of BL45XU

BL45XU was reconstructed to a macromolecular crystallography beamline using a microfocusing beam of a few to a few tens of microns. All the optical components such as the monochromator and focusing mirrors were replaced by new components (Fig. 1). The monochromator was replaced by a new one optimized for the beamline application energy range. A focusing optical system was also designed for use of a small focusing beam with a high flux. Ion pumps were adopted as the main pump of the transport channel. Reconstruction started in December 2018 and was completed in three months. The beamline will be opened for public use beginning in 2019A after a short commissioning period.

(1) Monochromator

Since the photon energy range was restricted between 6.5 keV and 16 keV, the mechanism was simplified (Fig. 2). The silicon 111 crystals and crystal holders were compatible with those of other beamlines. The rotation center of the Bragg angle stage did not correspond to the center of the second crystal. The positions of the beam footprints were shifted in accordance with the photon energies. Consequently, the long translation stage (Y1) was eliminated. Only three stages remained in the

Fig. 1. Remodeled optics in the optics hutch of BL45XU.

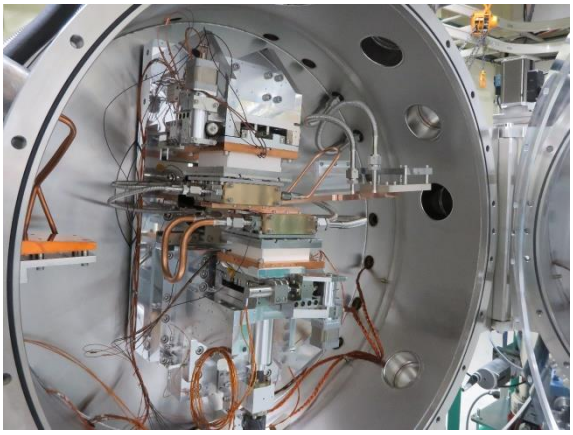

Fig. 2. Inside of the BL45XU monochromator.

vacuum chamber: a fine rotation stage for the first crystal, a tilt stage for the second crystal, and a translation stage for crystal gap adjustment.

(2) Focusing-mirror optics

High-flux micro-focusing mirrors, including mirror alignment mechanisms used under high-vacuum conditions, were designed for the illumination optics of the protein crystallography beamline for X-ray energies from 6.5 keV to 16 keV. A two-stage focus was employed only in the horizontal direction to obtain a micro-focusing beam with a minimum loss of the photon flux. The first horizontal focusing mirror (Mh1) was set at 40.4 m from the undulator light source to produce the first focus at 48.0 m from the source, where a secondary source slit was set to limit the first focus size. The second horizontal focusing mirror (Mh2) was set at 56.5 m from the source to produce a final focus on the sample position at 58.0 m from the source in the experimental hutch. In the vertical direction, a vertical focusing mirror (Mv) was set at 57.0 m from the source to directly produce a focus on the sample position.

Figure 3 shows the KB mirror manipulator for Mh2 and Mv. The focusing beam size on the sample can be adjusted between 5 μm and 100 μm, depending on the size of the sample protein crystals with a high photon flux of 10^{12}–10^{13} photons/s. The final focus size can be adjusted by changing the slit size at the first horizontal focus and the incident angle of the two mirrors (Mv and Mh2).

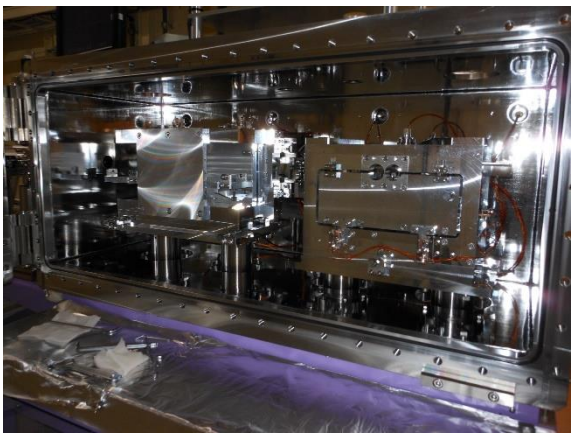

Fig. 3. KB mirror manipulator of BL45XU.

3. Radiation shielding for SPring-8 beamline

3-1. Radiation shielding hutches

The workflow was managed to replace the BL45XU hutches and other shielding-related components. A barrier-free automatic door was introduced for the first time in the SPring-8 beamline. It was also the first time that an automatic door was added to an existing hutch. In addition, malfunctioning sensors and electrical parts were exchanged at several beamlines.

3-2. Radiation-shielding calculations for the applications to the authority

The 44th change permission application contained radiation-dose calculations for the upper power revision of BL45XU. The 45th change permission application reviewed the dose estimations for the removal of the mirror of BL02B1. Moreover, the dose estimations were also reviewed for the movement of the downstream shutter of BL03XU.

3-3. Radiation leakage inspection at beamlines

The following beamlines were inspected: BL03XU, BL09XU, BL35XU, BL37XU, BL46XU (re-installation of local shield), BL10XU (exchange of insertion device), BL19LXU (change of FE slit), BL22XU (renewal of monochromator), BL24XU (conversion in the hutch), BL28B2 (movement of gamma stopper), BL28XU (exchange of gamma stopper), and BL29XU (exchange of collimator).

3-4. Radiation measurements and the development of methods

Maintenance of the GafChromic film–reading equipment was continued.

4. Beamlines of SACLA

Since September 2017, three beamlines of SACLA (BL1–BL3) have been operating in parallel (Fig. 4) [2]. The soft X-ray free-electron laser (SX-FEL) beamline (BL1) supplies femtosecond SX pulses with photon energies between 40 eV and 150 eV. This beamline has a dedicated 800-MeV linac (SCSS+) to operate independently at 60 Hz. Two hard X-ray FEL (XFEL) beamlines (BL2 and BL3) produce high-energy X-ray pulses in the range of 4–20 keV. The SACLA main linac drives these two XFEL beamlines simultaneously by switching an electron-beam route in a pulse-by-pulse manner. The fast-switching operation will also include a beam injection into the storage ring of SPring-8. The injection test started in FY2018. In addition to the effort to expand the availability of the FEL beamlines, SACLA has developed advanced operation schemes such as two-color XFEL generation [3] and reflection self-seeding [4]. Below the reflection self-seeding system, which has been available since FY2018, is described.

The reflection self-seeding system was established at BL3 to supply XFEL pulses with a much narrower bandwidth. In this system, a monochromatic X-ray pulse (seed pulse) is extracted from a pulse of self-amplified-spontaneous-emission (SASE) XFEL through a Bragg reflection in a channel-cut crystal of silicon at the middle of the undulator line. The first section of the undulator line generates the SASE XFEL pulse from an electron beam, while the second section amplifies the seed pulse through interactions with the electron beam. This system successfully produces nearly Fourier-transform-limited XFEL pulses with an average spectral brightness that is about six times higher than that of normal SASE XFEL pulses (Fig. 5). User operation of the self-seeding began in the 2018B term.

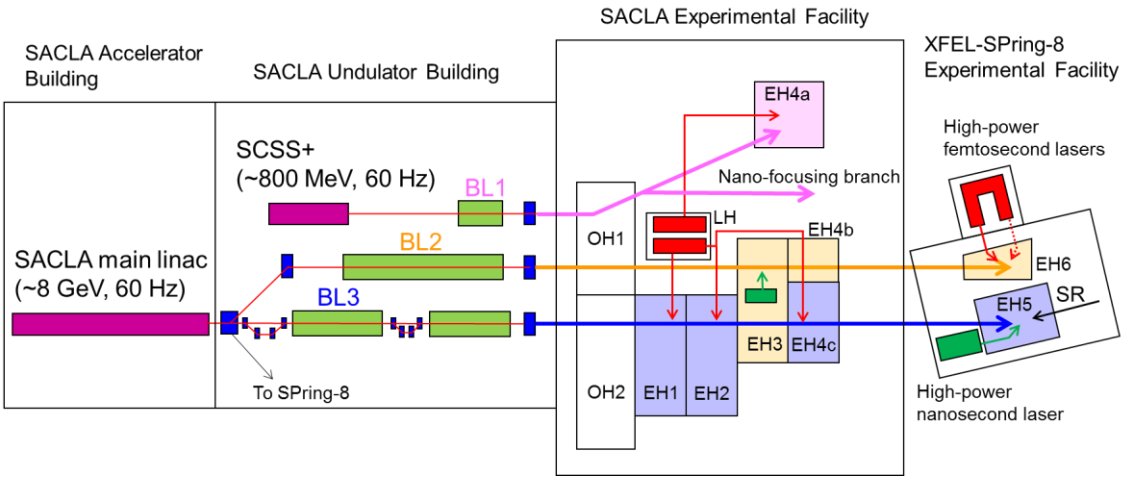

Fig. 4. Layout of the SACLA beamlines.

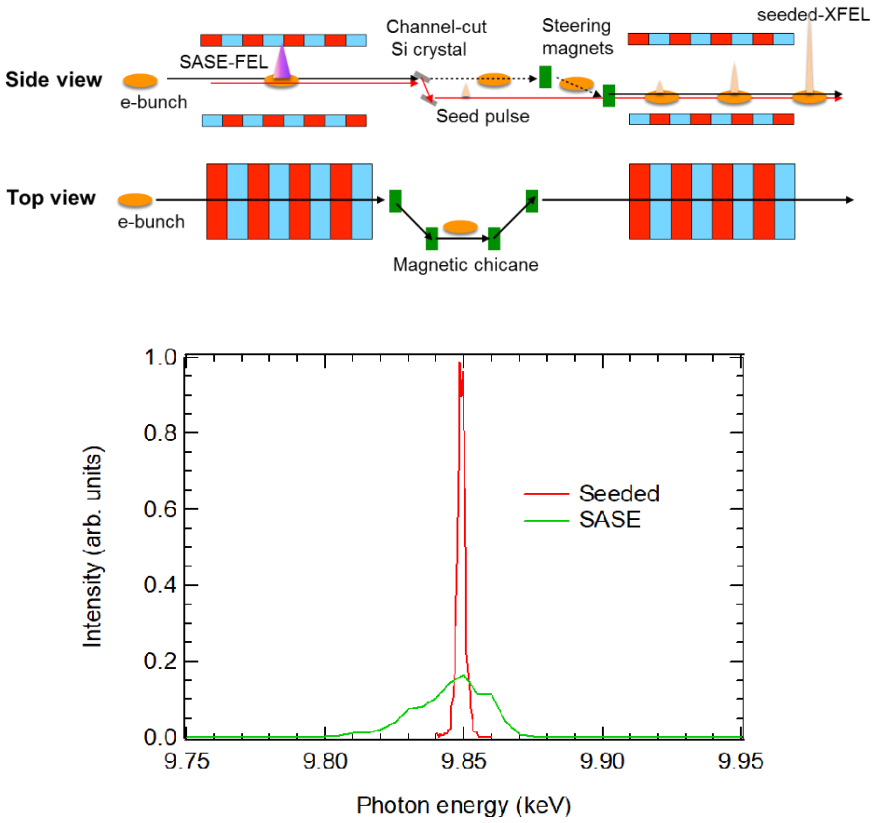

Fig. 5. Reflection self-seeding system of (upper) SACLA BL3 and (lower) averaged spectra of SASE XFEL (green) and seeded XFEL (red) [4].

Takashi Tanaka[*1], Sunao Takahashi[*1], Hirokatsu Yumoto[*1], Yasunori Senba[*1], Hiroshi Yamazaki[*1], Haruhiko Ohashi[*1], Kunikazu Takeshita[*1], Nobuteru Nariyama[*1], Shunji Goto[*1], Yuichi Inubushi[*2], Toshinori Yabuuchi[*2], Kensuke Tono[*2], and Makina Yabashi[*3]

[*1] Light source division, JASRI

[*2] XFEL Utilization Division, JASRI

[*3] XFEL Research and Development Division, RIKEN SPring-8 Center

References:

[1] S. Takahashi et al., Vacuum 155, 325-335 (2018).

[2] K. Tono et al, *J. Synchrotron Rad.* **26**, 595-602 (2019).

[3] T. Hara et al., *Nat. Commun.* **4**, 2919 (2013).

[4] I. Inoue et al., *Nat. Photon.* **13**, 319-323 (2019).